Articles

Effect of Drastic Sequence Alteration and D-Amino Acid Incorporation on the Membrane Binding Behavior of Lytic Peptides†

Niv Papo and Yechiel Shai*

Department of Biological Chemistry, The Weizmann Institute of Science, Rehovot 76100, Israel

Received January 7, 2004; Revised Manuscript Received February 26, 2004

ABSTRACT: The amphipathic α-helix is a common motif found in many cell lytic peptides including antimicrobial peptides. We have recently shown that significantly altering the amphipathic structure of a lytic peptide by reshuffling its sequence and/or replacing a few L-amino acids with their D-enantiomers did not significantly affect the antimicrobial activity of the peptides nor their ability to bind and permeate negatively charged (PE/PG) membranes. However, a pronounced effect was observed regarding their hemolytic activity and their ability to bind and permeate zwitterionic (PC/Cho) membranes. To shed light on these findings, here we used surface plasmon resonance (SPR) with mono- and bilayer membranes. We found that the L-amino acid (aa) peptides bound 10−25-fold stronger to PC/Cho bilayers compared with monolayers, whereas the diastereomers bound similarly to both membranes. A two-state reaction model analysis of the data indicated that this difference is due to the insertion of the L-aa peptides into the PC/Cho bilayers, whereas the diastereomers are surface-localized. In contrast, only an ∼2-fold difference was found with negatively charged membranes. Changes in the amphipathicity markedly affected only the insertion of the L-aa peptides into PC/Cho bilayers. Furthermore, whereas the all-L-aa peptides bound similarly to the PC/Cho and PE/PG membranes, the diastereomers bound ∼100-fold better to PE/PG compared with PC/Cho membranes, and selectivity was determined only in the first binding step. The effect of the peptides on the lipid order determined by using ATR-FTIR studies supported these findings. Besides shedding light on the mode of action of these peptides, the present study demonstrates SPR as a powerful tool to differentiate between non-cell-selective compared with bacteria-selective peptides, based on differences in their membrane binding behavior.

Interactions between bioactive polypeptides and phospholipid membranes play a key role in many cellular processes. A major family within bioactive peptides contains gene-encoded antimicrobial peptides isolated from almost all living organisms, including plants and humans, which are used in their defense and offense systems (*1*−*5*). Many of these peptides are able to lyse various types of cells (*6*, *7*) including bacteria, fungi, and mammalian cells. Regardless of their origin, most of these peptides are linear and relatively short, having less than 60 amino acids. Despite their remarkable sequence diversity, most of them have common features, namely, a net positive charge and a potential to form an amphipathic structure when bound to membranes. These properties are believed to be responsible for their ability to bind and disrupt negatively charged bacterial membranes better than the zwitterionic membranes composing the outer leaflet of mammalian cells (*5*, *8*−*10*). However, despite these similarities, antimicrobial peptides differ in their spectrum of activity. Some selectively kill microorganisms whereas others are also toxic to mammalian cells. Since the outer surface of mammalian membranes is predominantly zwitterionic, the interaction of lytic peptides with these membranes needs to be governed mostly by hydrophobic interactions; specifically, they need to penetrate into the hydrophobic core of the membrane. This is in contrast to bacteria-selective antimicrobial peptides, which interact mainly with the headgroups of negatively charged membranes.

To investigate the parameters involved in selective antimicrobial activity, we have synthesized and studied a new group of 15-mer peptides derived from an amphipathic α-helical lytic peptide composed of only Leu and Lys (*11*). These peptides either were synthesized in their all-L-aa form or contained both L- and D-amino acids (diastereomers). The amphipathic structure of some of these peptides was drastically altered. Importantly, we found that the all-L-aa peptides possessed both antimicrobial and hemolytic activities and preserved their potential to bind and permeate zwitterionic and negatively charged membranes. The activity was only partially reduced upon sequence alteration. However, all of the diastereomers showed antimicrobial but not hemolytic activity, concomitant with their ability to bind strongly and permeate only negatively charged membranes.

† This research was supported by European Community Project Number QLK2-2000-00411. Y.S. is the recipient of The Harold S. and Harriet B. Brady Professorial Chair in Cancer Research.

* To whom correspondence should be addressed. Tel: 972-8-9342711. Fax: 972-8-9344112. E-mail: Yechiel.Shai@ weizmann.ac.il.

10.1021/bi049944h CCC: $27.50
Published on Web 05/05/2004

To shed light on the mode of action of the all-L-aa peptides compared with their diastereomers, we utilized the surface plasmon resonance (SPR)[1] technique and ATR-FTIR spectroscopy. SPR has been used extensively to follow up in real time the binding behavior of a macromolecule in solution to another macromolecule immobilized on the surface (*12*). Unlike other methods, the SPR technique has the ability to monitor the amount of adsorbed complex with high sensitivity, therefore yielding important information about the kinetics of the binding event. A few studies were recently reported on the interaction of proteins or short peptides with phospholipid membranes. Most of them utilized hybrid lipid monolayers (using HPA sensor chip) (*13*, *14*), and only a few reported on the use of lipid bilayers (using the L1 sensor chip) (*15*), which comprise biological membranes. Recently, we have used monolayer and bilayer phospholipid membranes and have shown that the SPR technique enabled us to differentiate between pore-forming and non-pore-forming lytic peptides. Moreover, we showed that melittin formed pores only in zwitterionic membranes, whereas both melittin and the antimicrobial peptide magainin had a detergent-like effect on negatively charged membranes, similar to what has been predicted by other methods (*16*). Here we used the SPR technique to investigate the mode of membrane binding for all of the 15-mer peptides. In addition, we used ATR-FTIR spectroscopy to study the extent of membrane disruption by the peptides. The data revealed a clear difference between the mode of action of the all-L-aa peptides compared to their diastereomers, as well as differences between amphipathic and nonamphipathic peptides. The SPR studies were in agreement with the data obtained by using ATR-FTIR spectroscopy, thus demonstrating the power of the SPR technique for studying the mode of action of membrane-binding peptides. Furthermore, the common features found for hemolytic compared to nonhemolytic peptides should enable SPR to serve as a rapid method for screening potential antimicrobial peptides, urgently needed due to the increasing resistance of bacteria to the currently available antibiotics.

MATERIAL AND METHODS

Materials. 4-Methylbenzhydrylamine resin (BHA) and butyloxycarbonyl (Boc) amino acids were purchased from Calibochem-Novabiochem (La Jolla, CA). Other reagents used for peptide synthesis included trifluoroacetic acid (TFA; Sigma), *N*,*N*-diisopropylethylamine (DIEA; Aldrich), methylene chloride (peptide synthesis grade; Biolab), dimethylformamide (peptide synthesis grade; Biolab), piperidine (Merck, Darmstadt, Germany), and benzotriazolyl-*N*-oxytris-(dimethylamino)phosphonium hexafluorophosphate (BOP; Sigma). Trypsin, egg phosphatidylcholine (PC), egg phosphatidylglycerol (PG), phosphatidylethanolamine (PE) (type V, from *Escherichia coli*), *N*-octyl β-D-glucopyranoside (OG), and bovine serum albumin (BSA) were purchased from Sigma. Cholesterol (extra pure) was supplied by Merck (Darmstadt, Germany). All other reagents were of analytical grade. Buffers were prepared in double glass-distilled water.

Peptide Synthesis and Purification. Peptides were synthesized by a solid-phase method on 4-methylbenzhydrylamine resin (0.05 mequiv) (*17*) using the Boc strategy. Pardaxin was synthesized by a solid-phase method on butyloxycarbonyl-(amino acid)-(phenylacetamido)-methyl resin (0.05 mmol) (*17*). All resin-bound peptides were cleaved from the resins by hydrogen fluoride (HF) and, after HF evaporation and washing with dry ether, extracted with 50% acetonitrile/water. HF cleavage of the peptides bound to 4-methylbenzhydrylamine resin resulted in C-terminal amidated peptides. Each crude peptide contained one major peak, as revealed by RP-HPLC, that was 50−70% pure by weight. The peptides were further purified by RP-HPLC on a C_{18} reverse-phase Bio-Rad semipreparative column (250 × 10 mm, 300 Å pore size, 5 μm particle size). The column was eluted in 40 min using a linear gradient of 10−60% acetonitrile in water, both containing 0.05% TFA (v/v), at a flow rate of 1.8 mL/min. The purified peptides were shown to be homogeneous (>98%) by analytical HPLC. The peptides were further subjected to amino acid analysis and electrospray mass spectroscopy to confirm their composition and molecular weight.

Preparation of Small Unilamellar Vesicles (SUVs). SUVs were prepared by sonication of PC/Cho (10/1 w/w) or PE/PG (7/3 w/w) dispersions as previously described (*18*). Briefly, dry lipid mixtures were dissolved in a $CHCl_3$/MeOH mixture (2/1 v/v). The solvents were then evaporated under a stream of nitrogen, and the lipids (at a concentration of 7.2 mg/mL) were subjected to a vacuum for 1 h and then resuspended in the PBS by vortexing. The resulting lipid dispersions were then sonicated for 10 min in a bath-type sonicator (Bransonic B3-R sonicator; Branson Ultrasonics Corp., Danbury, CT) until clear. To avoid degradation of unsaturated lipids, sonication was performed at ~10 °C under a nitrogen atmosphere. Vesicles were visualized using a JEOL JEM 100B electron microscope (Japan Electron Optics Laboratory Co., Tokyo, Japan) as follows. A drop of vesicles was deposited on a carbon-coated grid and negatively stained with uranyl acetate. Examination of the grids demonstrated that the vesicles were unilamellar with an average diameter of 20−50 nm.

Binding Analysis by Surface Plasmon Resonance (SPR). SPR experiments were carried out with a BIAcore 3000 analytical system (Biacore, Uppsala, Sweden) using HPA and L1 sensor chips (BIAcore). The HPA sensor chip contains hydrophobic alkanethiol chains, which are covalently bound to its gold surface. A lipid heteromonolayer is created by introducing liposomes to the chip. On the other hand, The L1 sensor chip contains hydrophobic alkanethiol chains, which contain exposed polar headgroups. Thus, a lipid bilayer is being created by introducing liposomes to the chip. We performed a protocol as previously described by Mozsolits et al. (*13*). Briefly, the running buffer used for all experiments was PBS (pH 7.4). The washing solution was 40 mM *N*-octyl β-D-glucopyranoside. All solutions were freshly prepared, degassed, and filtered through 0.22 μm pores. The operating temperature was 25 °C. After cleaning as indicated by the manufacturers, the BIAcore X instrument was left running

[1] Abbreviations: ATR-FTIR, attenuated total reflectance Fourier transform infrared; BHA, 4-methylbenzhydrylamine resin; Boc, butyloxycarbonyl; HF, hydrogen fluoride; PBS, phosphate-buffered saline; PC, egg phosphatidylcholine; PE, *Escherichia coli* phosphatidylethanolamine; PG, egg phosphatidylglycerol; Cho, cholesterol; RP-HPLC, reverse-phase high-performance liquid chromatography; SUV, small unilamellar vesicles; TFA, trifluoroacetic acid; RU, response units; SPR, surface plasmon resonance.

overnight using Milli-Q water as eluent to thoroughly wash all liquid-handling parts of the instrument. The HPA (or L1) chip was then installed, and the alkanethiol surface was cleaned by an injection of the nonionic detergent *N*-octyl β-D-glucopyranoside (25 μL, 40 mM) at a flow rate of 5 μL/min. PC/Cho (10/1 w/w) and PE/PG (7/3 w/w) SUVs (80 μL, 0.5 mM) were then applied to the chip surface at a flow rate of 2 μL/min. To remove any multilamellar structures from the lipid surface, we increased the flow rate to 100 μL/min, which resulted in a stable baseline corresponding to the lipid monolayer (or bilayer in the case of L1) linked to the chip surface. The negative control BSA was injected (25 μL, 0.1 mg/μL in PBS) to confirm complete coverage of the nonspecific binding sites. The monolayer or bilayer linked to the chip surface was then used to study the peptide−membrane binding.

Peptide solutions (30 μL of PBS solution of 0.015 μM−100 mM peptide) were injected onto the lipid surface at a flow rate of 5 μL/min. PBS alone then replaced the peptide solution for 15 min to allow peptide dissociation. SPR detects changes in the reflective index of the surface layer of peptides and lipids in contact with the sensor chip. A sensorgram is obtained by plotting the SPR angle against time. This change in the angle is then translated to response units. Analysis of the peptide−lipid binding event was performed from a series of sensorgrams collected at different peptide concentrations. Our system reached binding equilibrium during sample injection, and therefore the affinity constant could be calculated from the relationship between the equilibrium binding response units (RU_{eq} or RU_{max}) and the peptide concentration (C) using a steady-state affinity model. The affinity constants were thus determined by nonlinear least-squares (NLLSQ) fitting using the equation:

$$RU(X) = K_A X RU_{max}/(1 + K_A X)$$

where X is the peptide concentration, RU_{max} is the maximal response unit (or equilibrium binding response), and K_A is the affinity constant. The affinity constants are defined as the ratio of the association and dissociation rate constants ($K_A = k_a/k_d$, with k_a and k_d having 1/M s and 1/s units, respectively).

The sensorgrams for each peptide−lipid bilayer interaction (L1 chip) were also analyzed by curve fitting using numerical integration analysis (*19*). The BIAevaluation software offers different reaction models to perform complete kinetic analyses of the peptide sensorgrams. One curve-fitting algorithm, the two-state reaction model, was chosen on the basis of what is known about the possible binding mechanisms of antimicrobial peptides. The data were fitted globally by simultaneously fitting the sensorgrams obtained at different peptide concentrations. The two-state reaction model was applied to each data set. This model describes two reaction steps (*13*) which, in terms of peptide−lipid interaction, may correspond to

$$P + L \underset{k_{d1}}{\overset{k_{a1}}{\leftrightarrows}} PL \underset{k_{d2}}{\overset{k_{a2}}{\leftrightarrows}} PL^*$$

where (1) peptide (P) binds to lipids (L) to give PL and (2) the complex PL changes to PL*, which cannot dissociate directly to P + L and which may correspond to partial insertion of the peptide into the lipid bilayer. The corresponding differential rate equations for this reaction model are represented by

$$dRU_1/dt = k_{a1}C_A(RU_{max} - RU_1 - RU_2) - k_{d1}RU_1 - k_{a2}RU_1 + k_{d2}RU_2$$

$$dRU_2/dt = k_{a2}RU_1 - k_{d2}RU_2$$

where RU_1 and RU_2 are the response units for the first and second steps, respectively, C_A is the peptide concentration, RU_{max} is the maximum peptide binding capacity (or equilibrium binding response), and k_{a1}, k_{d1}, k_{a2}, and k_{d2} are the association and dissociation rate constants for the first and second steps, respectively. While k_{a1} has 1/(M s) units, k_{d1}, k_{a2}, and k_{d2} have 1/s units; thus the total affinity constant for the all process, K, has M^{-1} units. We used χ^2 statistical tests to validate the model.

ATR-FTIR Measurements. Spectra were obtained with a Bruker equinox 55 FTIR spectrometer equipped with a deuterated triglyceride sulfate (DTGS) detector and coupled with an ATR device as previously described (*20*). During data acquisition, the spectrometer was continuously purged with dry N_2 to eliminate the spectral contribution of atmospheric water. Samples were prepared as previously described (*21*). Briefly, a mixture of PC/Cho or PE/PG (1 or 0.5 mg) alone or with the peptide (~40 μg) was deposited on a ZnSe horizontal ATR prism (80 × 7 mm). The aperture angle of 45° yielded 25 internal reflections. Lipid−peptide mixtures were prepared by dissolving them together in a 1/2 $MeOH/CH_2Cl_2$ mixture and drying under a stream of dry nitrogen while moving a Teflon bar back and forth along the ZnSe prism. Polarized spectra were recorded, and the respective pure phospholipid in each polarization was subtracted to yield the difference spectra. The background for each spectrum was a clean ZnSe prism. Hydration of the sample was achieved by introduction of excess deuterium oxide (^2H_2O) into a chamber placed on top the ZnSe prism in the ATR casting and incubation for 2 h prior to acquisition of spectra. H/D exchange was considered complete after total shift of the amide II band. Any contribution of ^2H_2O vapor to the absorbance spectra near the amide I peak region was eliminated by subtraction of the spectra of pure lipids equilibrated with ^2H_2O under the same conditions.

ATR-FTIR Data Analysis. Prior to curve fitting, a straight base line passing through the ordinates at 1700 and 1600 cm^{-1} was subtracted. To resolve overlapping bands, the spectra were processed using PEAKFITTM (Jandel Scientific, San Rafael, CA) software. Second-derivative spectra accompanied by 13-data-point Savitsky−Golay were calculated to identify the positions of the component bands in the spectra. These wavenumbers were used as initial parameters for curve fitting with Gaussian component peaks. Position, bandwidths, and amplitudes of the peaks were varied until (i) the resulting bands shifted by no more than 2 cm^{-1} from the initial parameters, (ii) all of the peaks had reasonable half-widths (<20−25 cm^{-1}), and (iii) good agreement between the calculated sum of all of the components and the experimental spectra was achieved ($r^2 > 0.99$). The relative contents of different secondary structure elements were estimated by dividing the areas of individual peaks, assigned to a specific second-

Table 1: Designations, Sequences, and Retention Times of the Peptides Investigated

peptide designation	sequence[a]	RP-HPLC retention time (min)
L-aa peptides		
amphipathic-1L	L K L L K K L L K K L L K L L-NH_2	24.23
scrambled-4L	K L K L L K L L K L L K L L K-NH_2	24.41
segregated-5L	K K K L L L L L L L L L K K K-NH_2	23.30
pardaxin	GFFALIPKIISSPLFKTLLSAVGSALSSSGGQE-COOH	24.27
diastereomers		
amphipathic-1D	L K **L** L K **K** L **L** **K** K L L **K** L L-NH_2	22.95
amphipathic-2D	L L **K** K L **L** K **L** **L** L K L **L** K K-NH_2	23.12
amphipathic-3D	L L **K** L L **K** K **L** **L** K K L **L** K L-NH_2	21.31
scrambled-4D	K L **K** L L **K** L **L** **K** L L K **L** L K-NH_2	23.02
segregated-5D	K K **K** L L **L** L **L** **L** L L L **K** K K-NH_2	25.05
segregated-6D	L L **L** L L **K** K **K** **K** K K L **L** L L-NH_2	26.98

[a] Amino acids underlined and in bold are D-enantiomers. All of the model peptides are amidated in their C-terminus.

ary structure, by the whole area of the resulting amide I band. The results of four independent experiments were averaged.

Analysis of the Polarized ATR-FTIR Spectra. The ATR electric fields of incident light were calculated as follows (*22*, *23*):

$$E_x = \frac{2\cos\theta\sqrt{\sin^2\theta - n_{21}^2}}{\sqrt{(1-n_{21}^2)[(1+n_{21}^2)\sin^2\theta - n_{21}^2]}}$$

$$E_y = \frac{2\cos\theta}{\sqrt{1-n_{21}^2}}$$

$$E_z = \frac{2\sin\theta\cos\theta}{\sqrt{(1-n_{21}^2)[(1+n_{21}^2)\sin^2\theta - n_{21}^2]}}$$

where θ is the angle of a light beam to the prism normal at the point of reflection (45°) and $n_{21} = n_2/n_1$ [n_1 and n_2 are the refractive indices of ZnSe (taken as 2.4) and the membrane sample (taken as 1.5), respectively]. Under these conditions, E_x, E_y, and E_z are 1.09, 1.81, and 2.32, respectively. The electric field components together with the dichroic ratio [defined as the ratio between absorption of parallel (to the membrane plane), A_p, and perpendicularly polarized incident light, A_s] are used to calculate the orientation order parameter, *f*, by the formula:

$$f = \frac{2(E_x^2 - R^{ATR}E_y^2 + E_z^2)}{h(3\cos^2\alpha - 1)(E_x^2 - R^{ATR}E_y^2 - 2E_z^2)}$$

Lipid order parameters were obtained from the symmetric (~2853 cm^{-1}) and antisymmetric (~2922 cm^{-1}) lipid stretching mode setting $\alpha = 90°$ (*23*).

RESULTS

Here we used SPR and ATR-FTIR spectroscopy to differentiate between the mode of action of an all-L-amino acid amphipathic peptide and its analogues in which the sequence was drastically altered, as well as their diastereomeric forms. The amino acid sequences of the peptides are shown in Table 1. Figure 1 shows a Schiffer and Edmundson (*24*) wheel structure of the parental amphipathic-1L. The biological activity of the peptides has been reported previously (*11*). Furthermore, we have determined previously the

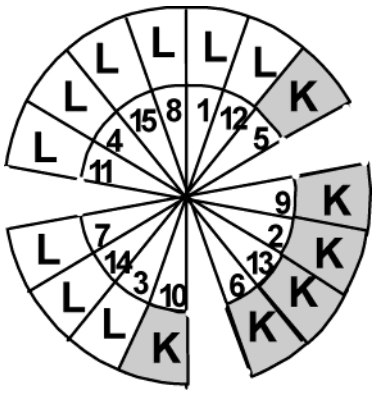

FIGURE 1: Schiffer−Edmundson wheel projection (*24*) of the parental model peptide amphipathic-1L. The gray background indicates hydrophilic amino acids. The empty background indicates hydrophobic amino acids.

structure of the peptides in PE/PG phospholipid membranes by using FTIR spectroscopy (*11*). Here we determined the structure of the peptides in PC/Cho membranes (Table 6). The data reveal that amphipathic-1L is indeed ~80% α-helix. Regarding amphipathic-1D, amphipathic-2D, and amphipathic-3D, they are also amphipathic. However, they do not form the classical α-helical structure but rather a distorded/3_{10}-helical structure. This type of 3_{10}-helical structure has an overall amphipathic character based on NMR spectroscopy (*25*). We also used pardaxin, a pore-forming peptide, as a reference peptide (*26*−*28*).

Peptide Partitioning and Insertion into Lipid Monolayers and Bilayers As Determined by Using SPR. (A) Steady-State Affinity Model for the Peptide's Insertion and Partitioning into the Membranes. The sensorgrams of the binding of amphipathic-1L and amphipathic-1D with PC/Cho mono- and bilayers and with PE/PG bilayers are given as examples in Figures 2 and 3. The sensorgram of the binding of the pore-forming peptide pardaxin with PE/PG bilayers is also shown in Figure 3. The sonograms revealed a markedly lower response upon the binding of the all-L-aa peptides and pardaxin with lipid monolayers compared with the bilayers. On the other hand, the diastereomeric peptides showed similar responses with lipid mono- and bilayers. This indicates that the inner layer contributes to the binding of the all-L-aa peptides but not to their diastereomers. Furthermore, all of the L-amino acid peptides showed a similar RU response in the PC and PE/PG monolayers or in the PC and PE/PG bilayers. In contrast, the diastereomers showed a

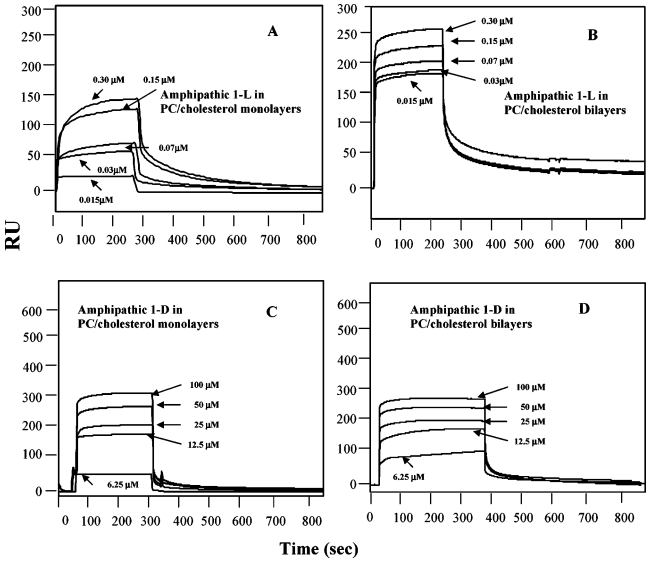

FIGURE 2: Sensorgrams of the binding of amphipathic-1L (panels A and B) and amphipathic-1D (panels C and D) with PC/Cho lipid monolayers (panels A and C) and bilayers (panels B and D). The concentrations used for amphipathic-1L were 0.015, 0.03, 0.07, 0.15, and 0.3 μM and for amphipathic-1D 6.25, 12.5, 25, 50, and 100 μM.

significantly lower response in the PC monolayers and bilayers compared with the PE/PG monolayers and bilayers, respectively. The sensorgrams also revealed that the intensity of the RU signals increased as a function of the peptide's concentration. This indicates that the amount of peptide bound to the lipids is proportional to the increase in peptide concentration. Our system reached binding equilibrium during the sample injection, and therefore the affinity constants could be calculated from the relationship between the equilibrium binding response (RU_{eq}) and the peptide's concentration (*C*) (Figure 4) using a steady-state affinity model. Tables 2 and 3 show the affinity constants of the peptides to zwitterionic and negatively charged membranes, as well as the ratio between the affinity constants in bilayers compared to monolayers. The data revealed that the affinity of the diastereomeric peptides to PE/PG membranes is ~50−100-fold higher than to PC/Cho membranes, similar to what has been obtained by other methods, e.g., magainin (*29*) and diastereomeric antimicrobial peptides (*30*). This indicates that electrostatic interactions play an important role in the affinity of the diastereomers to the membranes. In contrast, the affinity of the all-L-amino acid peptides is even slightly higher with PC/Cho compared to PE/PG phospholipid membranes, similar to what has been reported by other methods for other peptides, e.g., native melittin (*16*). This indicates that the affinity of the all-L-aa peptides to membranes is driven also by factors other than charge, i.e., helical content and the ease of formation of hydrophobic and hydrophilic faces independent of the structure of the peptide.

To estimate the contribution of the inner layer to the binding process, we examined the ratio between the affinity constants of the peptides in bilayers compared to monolayers. The values of the ratio $K_{A,bilayer}/K_{A,monolayer}$, listed in Table 2, demonstrate that the partition constants of the all-L-aa peptides with PC/Cho bilayers are ~10−25-fold higher than with PC/Cho monolayers, indicating that the inner leaflet contributes significantly to their binding to zwitterionic

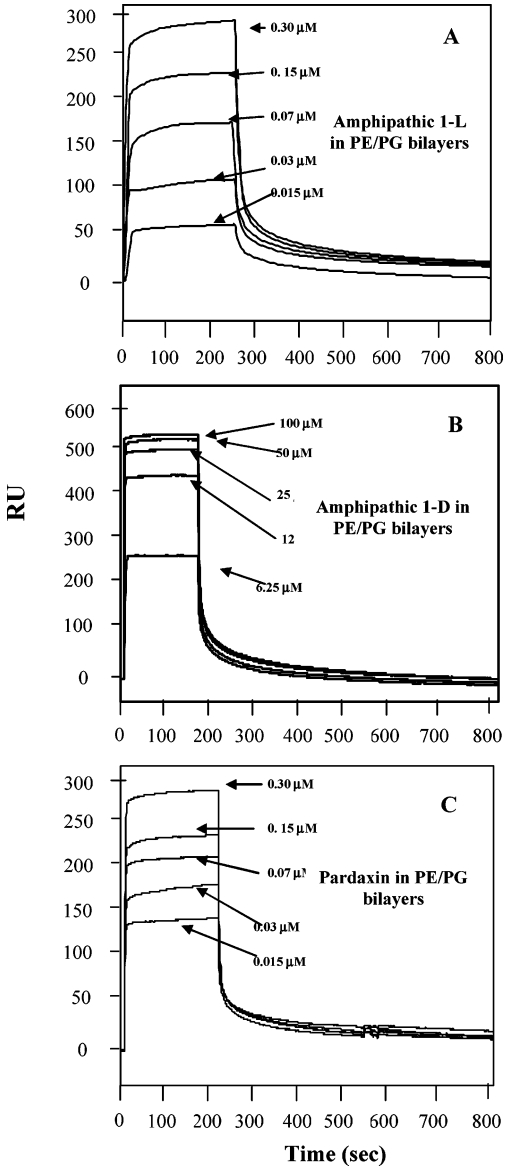

FIGURE 3: Sensorgrams of the binding of amphipathic-1L (panel A), amphipathic-1D (panel B), and pardaxin (panel C) with PE/PG lipid bilayers. The concentrations of amphipathic-1L and pardaxin were 0.015, 0.03, 0.07, 0.15, and 0.3 μM, and those of amphipathic-1D were 6.25, 12.5, 25, 50, and 100 μM.

membrane bilayers. A similar behavior is observed in PE/PG membranes;, however, the ratio is lower. The highest ratio was observed with the pore-forming peptide pardaxin with both types of membranes. In contrast, the binding of the diastereomers to PC/Cho bilayers is similar to their binding to monolayers (ratio = ~1) (Table 3), indicating that the inner leaflet does not contribute to their binding to PC/Cho bilayers. However, their binding to PE/PG bilayers is slightly higher (~2−3-fold) compared with monolayers, suggesting that the inner layer contributes slightly to the binding process, similarly to what was observed with the all-L-aa peptides in PE/PG membranes.

(B) Two-State Model for the Peptide's Interaction with Membranes. We employed numerical integration analysis that uses nonlinear analysis to fit an integrated rate equation directly to the sensorgrams (*13*). When fitting the peptide's sensorgrams globally (using different concentrations of peptide) with the simplest 1:1 Langmuir binding model, a

Table 2: Equilibrium Affinity Constants of the L-aa Peptides and Pardaxin in the Presence of PC/Cho and PE/PG Monolayers (HPA Chip) and Bilayers (L1 Chip) According to a Steady-State Affinity Model

	K_A in PC/Cho (10/1 w/w) ($\times 10^4\,M^{-1}$)			K_A in PE/PG (7/3 w/w) ($\times 10^4\,M^{-1}$)		
peptide designation	monolayer	bilayer	$K_{A,bilayer}/K_{A,monolayer}$	monolayer	bilayer	$K_{A,bilayer}/K_{A,monolayer}$
L-aa peptides						
amphipathic-1L	2.1 (±0.2)	34.8 (±2.2)	16.6	2.8 (±0.2)	10.8 (±1.4)	3.9
segregated-4L	1.4 (±0.1)	13.9 (±0.9)	9.9	2.5 (±0.2)	9.1 (±0.7)	3.6
segregated-5L	1.2 (±0.1)	14.5 (±1.0)	14.5	1.5 (±0.1)	3.6 (±0.2)	2.4
pardaxin	1.7 (±0.1)	42.9 (±2.3)	25.2	1.5 (±0.1)	16.0 (±1.1)	10.7

Table 3: Equilibrium Affinity Constants of the Diastereomeric Peptides in the Presence of PC/Cho and PE/PG Monolayers (HPA Chip) and Bilayers (L1 Chip) According to a Steady-State Affinity Model

	K_A in PC/Cho (10/1 w/w) ($\times 10^4\,M^{-1}$)			K_A in PE/PG (7/3 w/w) ($\times 10^4\,M^{-1}$)		
peptide designation	monolayer	bilayer	$K_{A,bilayer}/K_{A,monolayer}$	monolayer	bilayer	$K_{A,bilayer}/K_{A,monolayer}$
diastereomers						
amphipatic-1D	0.098 (±0.011)	0.105 (±0.010)	1.1	3.84 (±0.20)	6.60 (±0.56)	1.7
amphipatic-2D	0.100 (±0.013)	0.103 (±0.007)	1.0	4.68 (±0. 41)	8.04 (±0.77)	1.7
amphipatic-3D	0.110 (±0.009)	0.101 (±0.010)	0.9	5.45 (±0. 62)	10.41 (±1.11)	1.9
scrambled-4D	0.089 (±0.006)	0.089 (±0.004)	1.0	2.62 (±0. 06)	5.71 (±0.44)	2.2
segregated-5D	0.080 (±0.005)	0.084 (±0.009)	1.1	1.71 (±0.07)	4.29 (±0.29)	2.5
segregated-6D	0.086 (±0.006)	0.080 (±0.006)	0.9	1.91 (±0.22)	5.00 (±0.18)	2.6

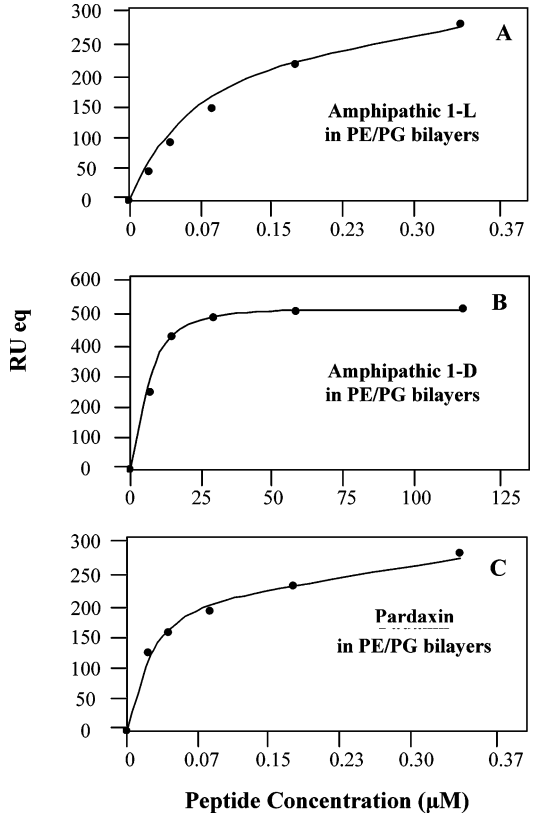

FIGURE 4: Relationship between the equilibrium binding response (RU_{eq}) and the peptide concentration (C) using BIAcore's steady-state affinity model with PE/PG lipid bilayers. The concentrations of amphipathic-1L (panel A) and pardaxin (panel C) were 0.015, 0.03, 0.07, 0.15, and 0.3 μM, and those of amphipathic-1D (panel B) were 6.25, 12.5, 25, 50, and 100 μM. The RU_{eq} for each concentration is the average of three independent measurements with a standard deviation not exceeding 10%.

poor fit was obtained ($\chi^2 > 100$), confirming that this model does not represent the lipid binding mechanism of the peptides. However, a significantly improved fit ($\chi^2 < 10$) was obtained using numerical integration of the two-state reaction model with the binding sensorgrams. This model describes two steps in the binding process between the peptides and lipids: the first step is the binding of the peptide to the surface, followed by a second step in which the peptide is inserted into the hydrophobic core of the membrane. A set of peptide sensorgrams with different peptide concentrations was used to estimate the kinetic parameters. The average values for the rate constants obtained from the two-state model analysis are listed in Tables 4 and 5 for the all-L-amino acid peptides and their diastereomers, respectively. The data are shown only for peptide−bilayer interactions (L1 chip). The results can be summarized as follows: (i) The affinity constants, K (Tables 4 and 5), determined by using the two-state model are similar to those obtained by directly fitting the data using a steady-state model (Tables 2 and 3), which further validates the two-state model as the appropriate one. Note that in the steady-state model there is no specific assumption on the kinetic behavior of the peptides. (ii) The amphipathic structure of a peptide is not a prerequisite for its affinity to the membrane in the first binding step, but rather in the second step. This is illustrated by the similar k_{a1} values obtained for the amphipathic and nonamphipathic all-L-aa-containing peptides (Table 4) and by the higher k_{a2} values for the amphipathic peptides compared with the nonamphipathic ones (including the diastereomeric counterparts; Table 5). (iii) All of the diastereomers interacted preferentially with anionic lipids compared with the zwitterionic ones in the first step but interacted similarly with both kinds of lipids in the second step. In contrast, all of the all-L-amino acid peptides interacted similarly with both kinds of lipids in the first step but interacted preferentially (four to eight times more) with zwitterionic lipids compared with the anionic ones in the second step. (iv) In all cases the contribution of the second step (K_2, insertion) was much smaller than the contribution of the first step (K_1, initial binding). The experiments were repeated three times with a standard deviation of 10%.

Secondary Structure of the Peptides in the PC/Cho Phospholipid Membrane As Determined by FTIR Spectroscopy. FTIR spectroscopy was used to determine the secondary structure of the peptides within the PC/Cho phospholipid membranes. Similar experiments were performed previously in the presence of PE/PG membranes (*11*). To resolve helical from unordered structures, we exchanged hydrogen with

Table 4: Association (k_{a1}, k_{a2}) and Dissociation (k_{d1}, k_{d2}) Rate Constants Determined by Numerical Integration Using the Two-State Reaction Model, the Affinity Constants, K_1 and K_2, for the First ($K_1 = k_{a1}/k_{d1}$) and Second ($K_2 = k_{a2}/k_{d2}$) Steps, Respectively, and the Affinity Constant (K) Determined as $(k_{a1}/k_{d1})(k_{a2}/k_{d2})$[a]

peptides	lipid	k_{a1} [1/(M s)]	k_{d1} (1/s)	K_1 ($\times 10^4$ M^{-1})	k_{a2} (1/s)	k_{d2} (1/s)	K_2	K ($\times 10^4$ M^{-1})
L-aa peptides								
amphipathic-1L	PC/Cho	18.2	0.0006	3.03	0.480	0.033	14.55	44.1
	PE/PG	18.1	0.0007	2.58	0.058	0.012	4.83	12.5
scrambled-4L	PC/Cho	17.8	0.0007	2.54	0.255	0.042	6.07	15.4
	PE/PG	18.3	0.0008	2.29	0.067	0.010	6.7	15.3
segregated-5L	PC/Cho	17.7	0.0007	2.53	0.242	0.039	6.2	15.7
	PE/PG	18.0	0.0006	3.0	0.038	0.021	1.81	5.4
pardaxin	PC/Cho	18.3	0.0006	3.05	0.362	0.019	19.1	58.1
	PE/PG	17.8	0.0006	2.96	0.107	0.013	8.23	24.4

[a] The peptides are in the presence of PC/Cho and PE/PG bilayers (L1 chip).

Table 5: Association (k_{a1}, k_{a2}) and Dissociation (k_{d1}, k_{d2}) Rate Constants Determined by Numerical Integration Using the Two-State Reaction Model, the Affinity Constants, K_1 and K_2, for the First ($K_1 = k_{a1}/k_{d1}$) and Second ($K_2 = k_{a2}/k_{d2}$) Steps, Respectively, and the Affinity Constant (K) Determined as $(k_{a1}/k_{d1})(k_{a2}/k_{d2})$[a]

peptides	lipid	k_{a1} [1/(M s)]	k_{d1} (1/s)	K_1 ($\times 10^4$ M^{-1})	k_{a2} (1/s)	k_{d2} (1/s)	K_2	K ($\times 10^4$ M^{-1})
diastereomers								
amphipathic-1D	PC/Cho	1.64	0.0091	0.018	0.042	0.022	1.9	0.04
	PE/PG	15.7	0.0007	2.240	0.054	0.024	2.3	5.71
amphipathic-2D	PC/Cho	1.34	0.0086	0.016	0.023	0.011	2.1	0.03
	PE/PG	13.1	0.0006	2.180	0.045	0.009	4.8	8.93
amphipathic-3D	PC/Cho	1.96	0.0073	0.029	0.038	0.013	2.9	0.11
	PE/PG	18.2	0.0006	3.030	0.065	0.015	4.3	11.8
scrambled-4D	PC/Cho	2.14	0.0011	0.194	0.003	0.003	0.9	0.21
	PE/PG	17.7	0.0007	2.530	0.003	0.003	1.3	3.03
segregated-5D	PC/Cho	1.98	0.0019	0.104	0.005	0.003	1.8	0.29
	PE/PG	12.8	0.0008	1.600	0.008	0.004	1.8	3.27
segregated-6D	PC/Cho	2.59	0.0023	0.113	0.009	0.005	1.7	0.23
	PE/PG	11.59	0.0009	1.290	0.009	0.003	2.7	3.21

[a] The peptides are in the presence of PC/Cho and PE/PG bilayers (L1 chip). The results are the average of three independent repetitions with a standard deviation of 10%.

deuterium, since the absorption of the random structure shifts to a higher extent than the α-helical component after deuteration. Therefore, we examined the IR spectra of the peptides after complete deuteration. Second derivatives, accompanied by 13-data-point Savitsky−Golay, were calculated to identify the positions of the component bands in the spectra (figure not shown). These wavenumbers were used as initial parameters for curve fitting with Gaussian component peaks. We assigned the different secondary structures to the various amide I regions similarly to what has been described for these peptides incorporated into PE/PG membranes (*11*). The derived structures shown in Table 6 are based on the following assignments: The amide I region from 1656 to 1670 cm^{-1} is characteristic of 3_{10}-helix or dynamic/distorted α-helix as was previously suggested in a study that examined structural changes in phospholipase A_2 (*31*). The assignment of the amide I region from 1656 to 1670 cm^{-1} to dynamic helix is based on studies that examined distorted α-helical structures (a_{II} helices) in bacteriorhodopsin and other proteins (*32*, *33*). These studies demonstrated that distorted α-helical structures are characterized by increased amide I frequencies compared with pure α-helical structures (1645−1654 cm^{-1}). The assignment of the amide I region between 1670 and 1680 cm^{-1} remains uncertain. Previous studies have correlated this region with β-turns (*34*), possibly sterically constrained non-hydrogen-bonded amide C═O groups within turns (*35*), or the high-frequency β-sheet component (*36*), which arises as a consequence of a transition dipole coupling (*37*).

Table 6: Peptide Structure As Determined by ATR-FTIR Spectroscopy from the Deconvolution of the Amide I Bands of the All-L and the Diastereomeric Peptides Incorporated into PC/Cho Multibilayers[a]

peptide designation	β-sheet + aggregated strands (%)	α-helix (%)	distorted/ 3_{10}-helix (%)
L-aa peptides			
amphipathic-1L	5 ± 1	80 ± 3	15 ± 1
scrambled-4L	65 ± 3	35 ± 2	
segregated-5L	70 ± 2	30 ± 2	
diastereomers			
amphipathic-1D	10 ± 1	40 ± 2	50 ± 3
amphipathic-2D	26 ± 2		74 ± 2
amphipathic-3D	25 ± 2		75 ± 2
scrambled-4D	43 ± 2		57 ± 3
segregated-5D	50 ± 3	40 ± 2	10 ± 1
segregated-6D	45 ± 2	30 ± 1	25 ± 2

[a] A 120/1 lipid/peptide molar ratio was used. The results are the average of three independent experiments.

The data reveal high similarities between the structures of the peptides in PC/Cho compared with their previously reported structures in PE/PG membranes (*11*). As expected, amphipathic-1L is predominantly α-helix (80%). In contrast, both scrambled-4L and segregated-5L are predominantly aggregated β-strands, with some contribution of an α-helical structure. Regarding the amphipathic diastereomers, they all adopt mainly distorted/3_{10}-helix with that of amphipathic-1D containing 40% α-helical structure. Interestingly, despite a difference in the distribution of Lys and Leu in the diastereomeric segregated-5D and -6D, both have similar

Table 7: ATR Dichroic Analysis of Phospholipid Multibilayers[a]

sample[a]	$\nu_{antisymmetric}(CH_2)$	
	R	*f*
PC/Cho	1.23	0.37
PC/Cho + amphipathic-1L	1.38	0.29
PC/Cho + scrambled-4L	1.38	0.28
PC/Cho + segregated-5L	1.39	0.28
PC/Cho + pardaxin	1.40	0.29
PC/Cho + amphipathic-1D	1.30	0.33
PC/Cho + amphipathic-2D	1.28	0.36
PC/Cho + amphipathic-3D	1.29	0.34
PC/Cho + scrambled-4D	1.25	0.36
PC/Cho + segregated-5D	1.30	0.33
PC/Cho + segregated-6D	1.30	0.33
PE/PG	1.27	0.30
PE/PG + amphipathic-1L	1.39	0.24
PE/PG + scrambled-4L	1.37	0.23
PE/PG + segregated-5L	1.37	0.25
PE/PG + pardaxin	1.42	0.20
PE/PG + amphipathic-1D	1.39	0.23
PE/PG + amphipathic-2D	1.37	0.23
PE/PG + amphipathic-3D	1.36	0.25
PE/PG + scrambled-4D	1.38	0.24
PE/PG + segregated-5D	1.35	0.24
PE/PG + segregated-6D	1.38	0.23

[a] The results are the average of three independent repetitions with a standard deviation of 10%.

structures, which is about 35% α-helix and 45% aggregated *β*-strands. Similar results were obtained when 1/60 and 1/120 peptide to lipid molar ratios were used.

Orientation of the Phospholipid Membranes and Effect of the Peptides on Phospholipid Acyl Chain Order. We used polarized ATR-FTIR spectroscopy to determine the orientation of the lipid membranes without bound peptides and the effect of the peptides on the acyl chain order. The symmetric [$\upsilon_{sym}(CH_2) \sim 2853$ cm^{-1}] and the antisymmetric [$\upsilon_{antisym}(CH_2) \sim 2922$ cm^{-1}] vibrations of lipid methylene C−H bonds are perpendicular to the molecular axis of a fully extended hydrocarbon chain. Thus, measurements of the dichroism of infrared light absorbance can reveal the order and orientation of the membrane sample relative to the prism surface. *R* values based on the stronger $\upsilon_{antisym}(CH_2)$ of PC/Cho (10/1 w/w, 0.5 mg) and PE/PG (7/3 w/w, 1 mg) multibilayers were 1.23 ± 0.02 and 1.27 ± 0.01, respectively (Table 7). On the basis of the dichroic ratio of lipid stretching, the corresponding orientation order parameter, *f*, was calculated. The data indicated that the phospholipid membrane is well ordered. The observed antisymmetric and symmetric peaks at ∼2922 and ∼2853 cm^{-1}, respectively, indicated that the membranes were predominantly in a liquid-crystalline phase (*23*, *38*), like biological cell membranes.

The effect of the peptides on the multibilayer acyl chains' order was estimated by comparing the CH_2-stretching dichroic ratio of pure phospholipid multibilayers with that in the presence of peptides. The *R* values and the corresponding order parameters, *f*, are summarized in Table 7. The data reveal that the incorporation of the diastereomers into PC/Cho membranes had a significantly smaller effect on the lipid order compared with the effect of the all-L-aa peptides. This supports the SPR data, indicating that the all-L-aa peptides are inserted into the zwitterionic membranes, whereas the diastereomers are not. Furthermore, similar to the findings in the SPR experiments, both the all-L-aa peptides and their diastereomers have similar effects on the acyl chain order of PE/PG membranes. Similar results were obtained when we used 1/60 or 1/120 peptide/lipid molar ratios.

DISCUSSION

We utilized SPR to follow real time kinetics of the peptide's binding to lipid monolayers and binding and insertion into lipid bilayers. Combined with ATR-FTIR spectroscopy, we shed light on the mode of action of a non-cell-selective lytic peptide, its analogues with altered sequences and structures, and their bacteria-selective diastereomers. Pardaxin, a natural pore-forming toxin, was used as a control peptide. The data support a two-step process: initial association with the outer surface of the membrane followed by an insertion step. Lytic peptides with differences in these steps are characterized by different biological functions.

Involvement of Electrostatic and Hydrophobic Forces in the Binding Process. Electrostatic forces contribute significantly to the binding of positively charged peptides to PE/PG membranes, whereas hydrophobic interactions contribute to the binding to both PC/holesterol and PE/PG membranes. In contrast to the all-L-aa peptides, which bound strongly and similarly to both PE/PG and PC/Cho, their corresponding diastereomers bound 50−100-fold better to PE/PG than to PC/Cho. Thus, electrostatic interactions appear to play an important role in the binding of the diastereomers to the PE/PG membranes. Note, however, that the contribution of electrostatic interaction to the binding of positively charged lytic peptides to PE/PG is ∼10-fold less than to the binding to PC/PG or PC/PS membranes (*39*, *40*). The strong binding to PE/PG is due to an ∼5−10-fold increase in the rate of association, K_{a1}, and an ∼10-fold decrease in the rate of dissociation, K_{d1}, compared with PC membranes (Table 5). The equilibrium binding affinity constants (Tables 2 and 3) observed for the different peptides correlate with their mode of action with monolayers and bilayers. The association rate constants, k_{a1} (Tables 4 and 5), of L-aa peptides for PC/Cho bilayers are significantly higher than the k_{a1} values of the corresponding diastereomers. Since the L-aa peptides and the diastereomers would have the same degree of cationicity and overall hydrophobicity, the observed association constants can be explained in terms of the structure of the peptides. Indeed, all of the L-aa peptides adopt either α-helical or aggregated *β*-strand structures, which allow better exposure of their hydrophobic faces to the hydrophobic core of the membrane. In support of this, previous studies have shown that the incorporation of four D-amino acids within the sequence of melittin reduced its affinity to PC membranes by ∼100-fold compared with native melittin (*41*). This is because of its flexible distorted/3_{10}-helical structure that does not form a classical amphipathic α-helical structure in the membrane. Thus, it prevents the formation of a well-defined hydrophobic face which facilitates binding to zwitterionic membranes.

Our results demonstrate the role of electrostatic interactions between the diastereomers and membranes only in the first binding step. This conclusion is supported by the finding that most of the difference in the binding constants between PC/Cho and the PE/PG membranes is due to differences in the K_1 values of the two-state model. Differences in the K_2 values are only marginal and are ∼2-fold to the most. In

contrast, the K_1 values of the all-L-aa peptides are practically similar, independent of the lipid type used. Note, however, that hydrophobic interactions contribute more in the second step in which the peptides insert into zwitterionic membranes. Peptides that favor a stable amphipathic structure in the membrane, i.e., amphipathic-1L and the pore-forming peptide pardaxin, have the highest K_2 values when bound to PC/Cho. In addition, a comparison between the all-L-aa helical peptide amphipathic-1L and its corresponding diastereomers with altered helical structures, namely, amphipathic-1D, -2D, and -3D, reveals up to an ~7-fold higher K_2 value for the all-L-aa peptide compared with the diastereomers when bound to PC/Cho (Tables 4 and 5). Note also that, with the all-L-aa peptides, the rate of association in the first step, k_{a1}, is the same for PC/Cho and PE/PG, but k_{a2} is about 3-fold higher for PC/Cho than for PE/PG (Table 4). A plausible explanation is the stronger association of the positively charged peptides with the negatively charged surface of PE/PG compared with a zwitterionic surface of PC/Cho. This binding makes it more difficult for the peptides to insert into the hydrophobic core of PE/PG. In contrast, since the binding of the diastereomers is predominantly electrostatically driven and takes place in the first step, the k_{a1} of each diastereomer is much higher for PE/PG compared with the PC/Cho membranes, but k_{a2} is the same for both types of lipids.

The biosensor and FTIR results presented here also correlate well with the biological activity of these peptides reported previously (*42*). More specifically, the low hemolytic activity of the diastereomers compared with the high hemolytic activity of the all-L-aa parental peptides correlates with a weak affinity of the diastereomers toward PC/Cho lipids compared with the all-L-aa peptides. Furthermore, the ATR-FTIR studies revealed that the diastereomers had only a slight effect on the lipid order of PC/Cho membranes compared with a stronger effect of the all-L-aa peptides (Table 7). Note also that the all-L-aa peptides and the corresponding diastereomers have a similar effect on the lipid order of PE/PG membranes (Table 6), in agreement with their similar antimicrobial activity (*11*).

Binding to Monolayers versus Bilayers: An Approach To Understand the Mechanism of Interaction. We followed up the binding of the peptides to both the monolayer and bilayer membranes and used a steady-state model to determine the corresponding binding constants. This allows examining the contribution of the inner layer of the membrane with regard to the binding properties of the peptides. This approach has been recently reported to differentiate between transmembrane pore formation by melittin versus membrane disruption by the antimicrobial peptide magainin (*40*). Here we have shown a marked difference between the mode of action of the L-aa peptides and their diastereomers. Significantly, we found an ~10−25-fold increase in the binding constant of the L-aa peptides to PC/Cho lipid bilayers compared with the monolayers. This indicates that the inner membrane contributes to the binding constants, or in other words, the L-aa peptides insert into the inner PC/Cho membrane. Further support for this notion comes from the data obtained by using the two-step model to fit the sensorgrams of the binding of the peptides to the bilayers. We found that the binding constant, K_1, which corresponds to the binding of the peptides to the surface of the bilayer (Table 4), is similar to the binding constant for the monolayers determined by the steady-state model (Table 2). In contrast, there was no increase in the binding constant of the diastereomers to PC/Cho bilayers compared to monolayers. The ratio between the binding constants in the two systems did not exceed ~1. This strongly suggests that the diastereomers do not insert into the hydrophobic core of the membrane and therefore they cannot form transmembrane pores. Note that a different situation was observed with PE/PG membranes. Tables 2 and 3 show only an ~2.5−4-fold increase in the binding of the L-aa peptides to lipid bilayers compared with the lipid monolayer and about ~2-fold in the case of the diastereomers. This suggests that the inner layer contributes only slightly to the binding process for all of the peptides. The only exception is the pore-forming pardaxin, in which there was an increase of ~11-fold in its binding to the PE/PG bilayers. This value is similar to that found for melittin in PE/PG (*40*). This suggests that pardaxin acts partially as a pore-forming peptide in negatively charged membranes as suggested previously (*28*, *43*, *44*) but partially also as a detergent, similarly to melittin (*16*). Indeed, although pardaxin has a net charge of +1 compared to +6 for melittin, they have significant homology at their N-terminal 22 aa pore-forming domain (*45*). In their experiments, White et al. (*46*) detected the release of encapsulated markers of different sizes from POPC and POPG vesicles induced by melittin. They showed that melittin is more active on POPC vesicles than POPG. Furthermore, melittin induced the release of encapsulated markers with defined sizes, suggesting that it forms pores in POPC vesicles. However, no size dependence was found with POPG vesicles, suggesting the existence of a detergent-like effect with these vesicles. They also suggested that melittin induces a "partial detergent-like" (partial "carpet") effect in which peptide aggregates cause local structural instabilities and fluctuations equivalent to transient pores. Similar structures were also described as transient pores in toroidal pore formation and the carpet mechanism (review in ref *46*). Therefore, our data suggest that the mode of action of pardaxin in PE/PG membranes is as an intermediate (Figure 5C) between the "pore formation" (Figure 5D) and "carpet-like" (Figure 5B) mechanisms. It is possible that a similar "partial carpet" mechanism holds for the all-L-aa peptides with PC/Cho membranes (Figure 5C). This is because 15 amino acids are not sufficient to span the membrane. Indeed, on the basis of the FTIR studies, the amphipathic-1L is predominantly α-helix, and both scrambled-4L and segregated-5L adopt about one-third α-helical structure and about two-thirds β-aggregates, both of which should have an amphipathic organization. In between, the diastereomers as well as their all-L-amino acid counterparts are only partially inserted into the PE/PG bilayers. This is supported by the slightly higher K_A values with the PE/PG bilayers compared with the monolayers and the low K_2 values with bilayers obtained by the two-state model (Tables 3 and 5). The model, described in Figure 5C, resembles the one proposed recently for the interaction of the 15-aa gramicidin with membranes (*47*).

Although only a few detailed studies were conducted with BIAcore, all of which were done by using either monolayers alone or bilayers alone, there is agreement between them and other methods used. For example, Wang et al. determined K_A values of $\sim 10^4$ for the binding of cecropin B, a natural antimicrobial peptide, to PC/PA monolayers (*14*).

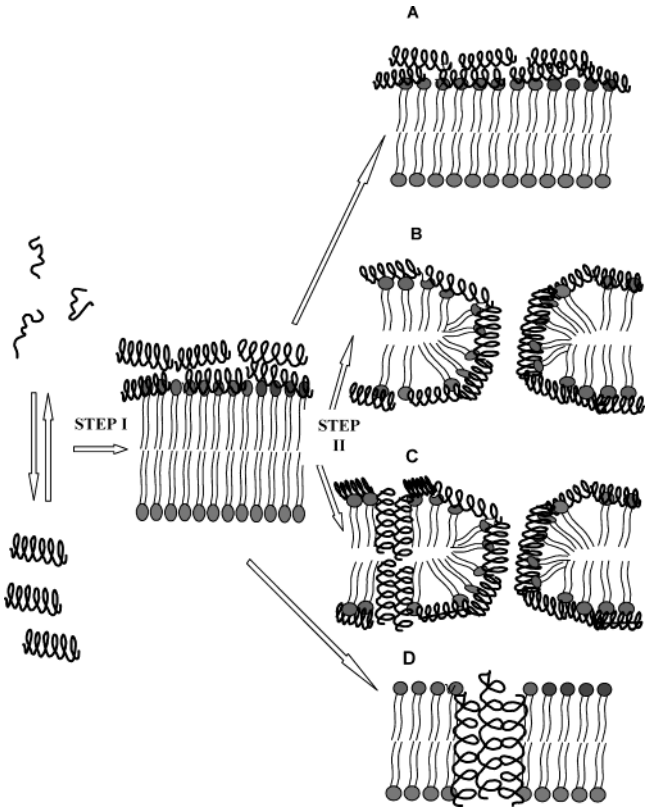

FIGURE 5: Schematic representation of the different possible mechanisms of membrane lysis by the peptides. Peptides bind in the first step predominantly by electrostatic interactions in the case of the diastereomers and by both electrostatic and hydrophobic interaction in the case of the L-aa peptides and align parallel to the outer membrane surface. Increasing peptide concentration results in different effects depending upon the peptide: (i) With regard to the diastereomers interacting with PC/Cho membranes (panel A), the peptides remain predominantly aligned parallel to the outer membrane surface without disturbing the membrane structure. (ii) With regard to all diastereomers and all-L peptides with PE/PG membranes (panel B), the peptides act via the carpet mechanism to induce micellization, which may include also the formation of toroidal-like pores (*5*, *8*, *16*, *52*, *53*). (iii) With regard to both amphipathic and nonamphipathic all-L peptides binding to zwitterionic and PE/PG membranes and pardaxin binding to PE/PG membranes, both "carpet-like" and "pore-forming" mechanisms might be involved (panel C). (iv) With regard to pardaxin binding to PC/Cho membranes (panel D), the peptide inserts deeply into the hydrocarbon region of the target cell membrane and forms transmembrane pores via the "barrel-stave" mechanism (*54*).

This value is similar to that obtained for our diastereomers with PE/PG monolayers (Table 3). In another study Mozsolits et al. found that magainin bound to DMPG monlayers ~100-fold better than to DMPC (*13*), similarly to what we found here with the diastereomers using monolayers (determined by a steady-state model) or in the first binding step using the two-step model. Overall, the binding constants obtained by using the BIAcore biosensor are similar to those values obtained by using different techniques such as equilibrium dialysis, centrifugation, high-sensitivity isothermal titration calorimetry, circular dichroism, and fluorescence (*30*, *39*, *41*, *48*−*51*).

In summary, this study clearly enables differentiating between the mode of action of an amphipathic α-helical lytic peptide, its sequence-altered analogues, and their diastereomers. Their mode of action shed light on their ability to lyse target cells in a specific or nonspecific manner. Furthermore, we demonstrated that the SPR technology allows not only determination of the binding constants, as has been reported previously, but also differentiation between two major steps: membrane binding and membrane insertion. Knowing these two steps enables determining whether a particular membrane-active peptide forms pores and destabilizes the membrane via the carpet mechanism or via another yet unclear intermediate between these two modes of actions. Furthermore, the finding that the binding constants calculated by a steady-state model are practically equal to those calculated by the two state model, and that both are in agreement with values determined by other methods, greatly supports the accuracy of the SPR technology in studying peptide−lipid interactions. Similar studies should assist in the rapid screening of cell-selective antimicrobial peptides urgently needed due to the increasing resistance of harmful microorganisms to the currently available antibiotics.

REFERENCES

1. Steiner, H., Hultmark, D., Engstrom, A., Bennich, H., and Boman, H. G. (1981) Sequence and specificity of two antibacterial proteins involved in insect immunity, *Nature 292*, 246−248.
2. Zasloff, M. (1987) Magainins, a class of antimicrobial peptides from Xenopus skin: isolation, characterization of two active forms, and partial cDNA sequence of a precursor, *Proc. Natl. Acad. Sci. U.S.A. 84*, 5449−5453.
3. Mor, A., Nguyen, V. H., Delfour, A., Migliore, S. D., and Nicolas, P. (1991) Isolation, amino acid sequence, and synthesis of dermaseptin, a novel antimicrobial peptide of amphibian skin, *Biochemistry 30*, 8824−8830.
4. Falla, T. J., Karunaratne, D. N., and Hancock, R. E. W. (1996) Mode of action of the antimicrobial peptide indolicidin, *J. Biol. Chem. 271*, 19298−19303.
5. Shai, Y. (1999) Mechanism of the binding, insertion and destabilization of phospholipid bilayer membranes by alpha-helical antimicrobial and cell nonselective membrane-lytic peptides, *Biochim. Biophys. Acta 1462*, 55−70.
6. Boman, H. G. (1995) Peptide antibiotics and their role in innate immunity, *Annu. Rev. Immunol. 13*, 61−92.
7. Zasloff, M. (2002) Antimicrobial peptides of multicellular organisms, *Nature 415*, 389−395.
8. Matsuzaki, K. (1999) Why and how are peptide-lipid unteractions utilized for self-defense? Magainins and tachyplesins as archyetypes, *Biochim. Biophys. Acta 1462*, 1−10.
9. Tossi, A., Sandri, L., and Giangaspero, A. (2000) Amphipathic, alpha-helical antimicrobial peptides, *Biopolymers 55*, 4−30.
10. Hancock, R. E., and Rozek, A. (2002) Role of membranes in the activities of antimicrobial cationic peptides, *FEMS Microbiol. Lett. 206*, 143−149.
11. Papo, N., Oren, Z., Pag, U., Sahl, H. G., and Shai, Y. (2002) The consequence of sequence alteration of an amphipathic alpha-helical antimicrobial peptide and its diastereomers, *J. Biol. Chem. 277*, 33913−33921.
12. Hall, D. (2001) Use of optical biosensors for the study of mechanistically concerted surface adsorption processes, *Anal. Biochem. 288*, 109−125.
13. Mozsolits, H., Wirth, H. J., Werkmeister, J., and Aguilar, M. I. (2001) Analysis of antimicrobial peptide interactions with hybrid bilayer membrane systems using surface plasmon resonance, *Biochim. Biophys. Acta 1512*, 64−76.
14. Wang, W., Smith, D. K., Moulding, K., and Chen, H. M. (1998) The dependence of membrane permeability by the antibacterial peptide cecropin B and its analogues, CB-1 and CB-3, on liposomes of different composition, *J. Biol. Chem. 273*, 27438−27448.
15. Mozsolits, H., and Aguilar, M. I. (2002) Surface plasmon resonance spectroscopy: An emerging tool for the study of peptide-membrane interactions, *Biopolymers 66*, 3−18.
16. Ladokhin, A. S., and White, S. H. (2001) 'Detergent-like' permeabilization of anionic lipid vesicles by melittin, *Biochim. Biophys. Acta 1514*, 253−260.

17. Merrifield, R. B., Vizioli, L. D., and Boman, H. G. (1982) Synthesis of the antibacterial peptide cecropin A (1−33), *Biochemistry 21*, 5020−5031.
18. Gazit, E., Lee, W. J., Brey, P. T., and Shai, Y. (1994) Mode of action of the antibacterial cecropin B2: a spectrofluorometric study, *Biochemistry 33*, 10681−10692.
19. Morton, T. A., Myszka, D. G., and Chaiken, I. M. (1995) Interpreting complex binding kinetics from optical biosensors: a comparison of analysis by linearization, the integrated rate equation, and numerical integration, *Anal. Biochem. 227*, 176−185.
20. Oren, Z., and Shai, Y. (2000) Cyclization of a cytolytic amphipathic alpha-helical peptide and its diastereomer: effect on structure, interaction with model membranes, and biological function, *Biochemistry 39*, 6103−6114.
21. Gazit, E., Miller, I. R., Biggin, P. C., Sansom, M. S. P., and Shai, Y. (1996) Structure and orientation of the mammalian antibacterial peptide cecropin P1 within phospholipid membranes, *J. Mol. Biol. 258*, 860−870.
22. Harrick, N. J. (1967) *Internal Reflection Spectroscopy*, Interscience, New York.
23. Ishiguro, R., Kimura, N., and Takahashi, S. (1993) Orientation of fusion-active synthetic peptides in phospholipid bilayers: determination by Fourier transform infrared spectroscopy, *Biochemistry 32*, 9792−9797.
24. Schiffer, M., and Edmundson, A. B. (1967) Use of helical wheels to represent the structures of protein and to identify segments with helical potential, *Biophys. J. 7*, 121−135.
25. Oren, Z., Ramesh, J., Avrahami, D., Suryaprakash, N., Shai, Y., and Jelinek, R. (2002) Structures and mode of membrane interaction of a short alpha helical lytic peptide and its diastereomer determined by NMR, FTIR, and fluorescence spectroscopy, *Eur. J. Biochem. 269*, 3869−3880.
26. Shai, Y., Hadari, Y. R., and Finkels, A. (1991) pH-dependent pore formation properties of pardaxin analogues, *J. Biol. Chem. 266*, 22346−22354.
27. Saberwal, G., and Nagaraj, R. (1993) Interaction of hydrophobic peptides with model membranes: slow binding to membranes and not subtle variations in pore structure is responsible for the gradual release of entrapped solutes, *Biochim. Biophys. Acta 1151*, 43−50.
28. Hallock, K. J., Lee, D. K., Omnaas, J., Mosberg, H. I., and Ramamoorthy, A. (2002) Membrane composition determines pardaxin's mechanism of lipid bilayer disruption, *Biophys. J. 83*, 1004−1013.
29. Matsuzaki, K., Murase, O., Fujii, N., and Miyajima, K. (1995) Translocation of a channel-forming antimicrobial peptide, magainin 2, across lipid bilayers by forming a pore, *Biochemistry 34*, 6521−6526.
30. Oren, Z., and Shai, Y. (1997) Selective lysis of bacteria but not mammalian cells by diastereomers of melittin: structure−function study, *Biochemistry 36*, 1826−1835.
31. Tatulian, S. A., Biltonen, R. L., and Tamm, L. K. (1997) Structural changes in a secretory phospholipase A2 induced by membrane binding: a clue to interfacial activation?, *J. Mol. Biol. 268*, 809−815.
32. Rothschild, K. J., and Clark, N. A. (1979) Anomalous amide I infrared absorption of purple membrane, *Science 204*, 311−312.
33. Dwivedi, A. M., and Krimm, S. (1984) Vibrational analysis of peptides, polypeptides, and proteins. XVII. conformational sensitivity of the alpha-helix spectrum: alpha-poly(L-alanine), *Biopolymers 23*, 923−943.
34. Pezolet, M., Bonenfant, S., Dousscau, F., and Papineau, Y. (1992) *FEBS Lett. 299*, 247−250.
35. Mantsch, H. H., Perczel, A., Hollosi, M., and Fasman, G. D. (1993) Characterization of beta-turns in cyclic hexapeptides in solution by Fourier transform IR spectroscopy, *Biopolymers 33*, 201−207.
36. Byler, D. M., and Susi, H. (1986) Examination of the secondary structure of proteins by deconvolved Fourier transform infrared spectroscopy, *Biopolymers 25*, 469−487.
37. Miyazawa, T. (1960) The characteristic band of secondary amides at 3000 cm^{-1}, *J. Mol. Spectrosc. 4*, 168−172.
38. Cameron, D. G., Casal, H. L., Gudgin, E. F., and Mantsch, H. H. (1980) The gel phase of dipalmitoyl phosphatidylcholine. An infrared characterization of the acyl chain packing, *Biochim. Biophys. Acta 596*, 463−467.
39. Jin, Y., Mozsolits, H., Hammer, J., Zmuda, E., Zhu, F., Zhang, Y., Aguilar, M. I., and Blazyk, J. (2003) Influence of tryptophan on lipid binding of linear amphipathic cationic antimicrobial peptides, *Biochemistry 42*, 9395−9405.
40. Papo, N., and Shai, Y. (2003) Exploring peptide membrane interaction using surface plasmon resonance: differentiation between pore formation versus membrane disruption by lytic peptides, *Biochemistry 42*, 458−466.
41. Ladokhin, A. S., and White, S. H. (1999) Folding of amphipathic alpha-helices on membranes: energetics of helix formation by melittin, *J. Mol. Biol. 285*, 1363−1369.
42. Papo, N., Shahar, M., Eisenbach, L., and Shai, Y. (2003) A novel lytic peptide composed of D, L amino acids selectively kills cancer cells in culture and in mice, *J. Biol. Chem. 278*, 21018−21023.
43. Rapaport, D., and Shai, Y. (1992) Aggregation and organization of pardaxin in phospholipid membranes. A fluorescence energy transfer study, *J. Biol. Chem. 267*, 6502−6509.
44. Rapaport, D., Peled, R., Nir, S., and Y., S. (1996) Reversible Surface Aggregation in Pore Formation by Pardaxin, *Biophys. J. 70*, 2502−2512.
45. Thompson, S. A., Tachibana, K., Nakanishi, K., and Kubota, I. (1986) Melittin-Like Peptides from the Shark-Repelling Defense Secretion of the Sole *Pardachirus pavoninus*, *Science 233*, 341−343.
46. Shai, Y., and Oren, Z. (2001) From "carpet" mechanism to de-novo designed diastereomeric cell-selective antimicrobial peptides, *Peptides 22*, 1629−1641.
47. Bransburg-Zabary, S., Kessel, A., Gutman, M., and Ben-Tal, N. (2002) Stability of an ion channel in lipid bilayers: implicit solvent model calculations with gramicidin, *Biochemistry 41*, 6946−6954.
48. Ben-Tal, N., Ben-Shaul, A., Nicholls, A., and Honig, B. (1996) Free-energy determinants of alpha-helix insertion into lipid bilayers, *Biophys. J. 70*, 1803−1812.
49. Ben-Tal, N., Honig, B., Peitzsch, R. M., Denisov, G., and McLaughlin, S. (1996) Binding of small basic peptides to membranes containing acidic lipids: theoretical models and experimental results, *Biophys. J. 71*, 561−575.
50. Beschiaschvili, G., and Seelig, J. (1990) Melittin binding to mixed phosphatidylglycerol/phosphatidylcholine membranes, *Biochemistry 29*, 52−58.
51. Epand, R. F., Lehrer, R. I., Waring, A., Wang, W., Maget-Dana, R., Lelievre, D., and Epand, R. M. (2003) Direct comparison of membrane interactions of model peptides composed of only Leu and Lys residues, *Biopolymers 71*, 2−16.
52. Pouny, Y., Rapaport, D., Mor, A., Nicolas, P., and Shai, Y. (1992) Interaction of antimicrobial dermaseptin and its fluorescently labeled analogues with phospholipid membranes, *Biochemistry 31*, 12416−12423.
53. Huang, H. W. (2000) Action of antimicrobial peptides: two-state model, *Biochemistry 39*, 8347−8352.
54. Ehrenstein, G., and Lecar, H. (1977) Electrically gated ionic channels in lipid bilayers, *Q. Rev. Biophys. 10*, 1−34.

BI049944H